

# Modeling and Predicting Transistor Aging under Workload Dependency using Machine Learning

Paul R. Genssler, *Member, IEEE*, Hamza E. Barkam, *Member, IEEE*, Karthik Pandaram, Mohsen Imani, *Member, IEEE* and Hussam Amrouch, *Member, IEEE*

**Abstract**—The pivotal issue of reliability is one of colossal concern for circuit designers. The driving force is transistor aging, dependent on operating voltage and workload. At the design time, it is difficult to estimate close-to-the-edge guardbands that keep aging effects during the lifetime at bay. This is because the foundry does not share its calibrated physics-based models, comprised of highly confidential technology and material parameters. However, the unmonitored yet necessary overestimation of degradation amounts to a performance decline, which could be preventable. Furthermore, these physics-based models are exceptionally computationally complex. The costs of modeling millions of individual transistors at design time can be evidently exorbitant. We propose the revolutionizing prospect of a machine learning model trained to replicate the physics-based model, such that no confidential parameters are disclosed. This effectual workaround is fully accessible to circuit designers for the purposes of design optimization. We demonstrate the models' ability to generalize by training on data from one circuit and applying it successfully to a benchmark circuit. The mean relative error is as low as 1.7%, with a speedup of up to 20X. Circuit designers, for the first time ever, will have ease of access to a high-precision aging model, which is paramount for efficient designs. This work is a promising step in the direction of bridging the wide gulf between the foundry and circuit designers.

**Index Terms**—Circuit Reliability, Transistor Aging, Degradation, Machine Learning.

## I. INTRODUCTION

**R**ELIABILITY is a major concern in today's circuits. As CMOS scaling reaches the atomic level, the impact of degradation effects on the reliability becomes stronger [1]. Aging is the most dominating effect and changes the transistor's properties like the threshold voltage  $V_{th}$ . Consequently, it can cause permanent failures in a circuit. Even before such failures, aging indirectly impacts the circuit's timing and hinders performance improvements. The negative bias temperature instability (NBTI) aging mechanism is responsible for the highest degradation [2]. During regular transistor operation, Si-H bonds at the Si-SiO<sub>2</sub> interface might be broken and annealed. Additionally, charges are captured and emitted in the oxide vacancies at the interface layer. Over time, these defects accumulate and manifest themselves as a shift in  $V_{th}$ , referred to as  $\Delta V_{th}$ . The induced increase in the propagation delay of the logic gates can cause timing violations.

Paul R. Genssler, Karthik Pandaram, and Hussam Amrouch are with the Chair of Semiconductor Test and Reliability (STAR), University of Stuttgart, Stuttgart 70569, Germany. E-mail: {genssler, amrouch}@iti.uni-stuttgart.de, st174730@stud.uni-stuttgart.de. Hamza E. Barkam and Mohsen Imani are with the Bio-Inspired Architecture and Systems (BIASLab), UC Irvine, California, USA. E-mail: {herrahmo, m.imani}@uci.edu.

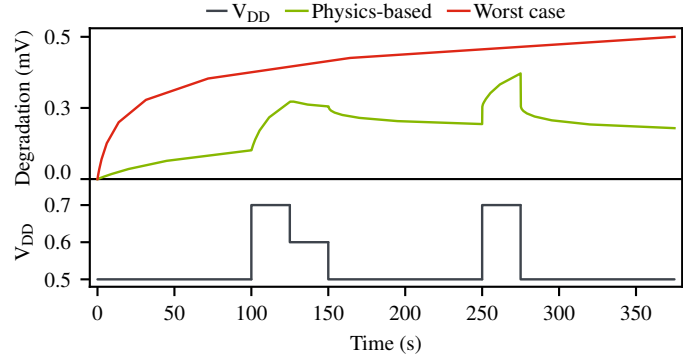


Fig. 1. Worst-case models are typically employed in the industry. For transistor aging, they assume constant stress and thus the highest possible degradation (red). Physics-based models are far more accurate because they take the input waveform and recovery effects into account.

To prevent such timing violations and ensure the circuit performs as specified during its entire projected lifetime, timing guardbands are added during the design phase. Such additional slack compensates for the reduced switching speed of aged transistors. The design challenge is to balance such guardbands between too pessimistic, reducing the circuit's performance, and too optimistic, increasing the risk of premature failures. To find an optimal guardband (i.e. small, yet sufficient), the aging-induced  $\Delta V_{th}$  has to be accurately estimated. Aging models are required to abstract the underlying physical behaviors, take technology parameters, stress patterns, and voltages into account, and predict the evolution of  $\Delta V_{th}$  over time. Only with such models can designers make informed and proper decisions on the guardband of every transistor.

Physics-based aging models capture the *dynamics* of the fundamental physical behavior and chemical reactions inside the transistors. Complex differential equations take the material and technology dependent parameters into account. This makes the model capable of capturing recovery effects, where  $V_{th}$  is indeed reduced as shown in Fig. 1. During low-stress phases, the defects are partially healed and  $V_{th}$  recovers [3]. The supply voltage  $V_{DD}$  is dynamic, creating such phases, changes over time, and is typically defined through the workload of the circuit. To capture these voltage dynamics, an aging model has to process such a voltage waveform. Worst-case aging models are not capable of this. They are created by fitting measurements of constant voltage stress on a transistor. Hence, they cannot model the physics of voltage dynamics and recovery effects. To process a voltage waveform, the highest voltage is applied for the whole duration of the voltage waveform. Consequently,

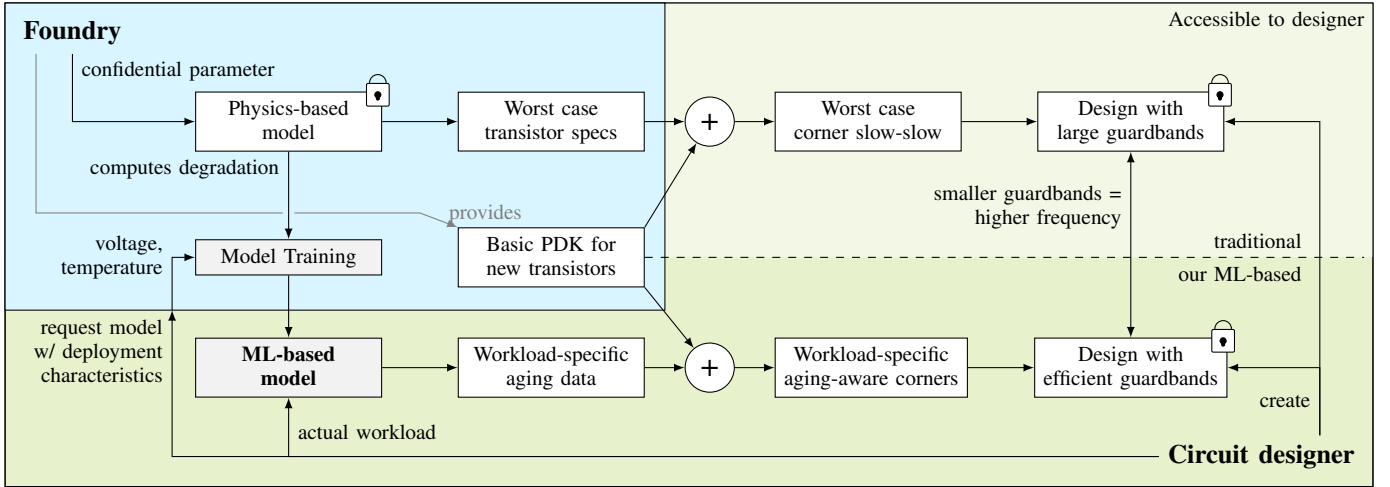


Fig. 2. Typically, circuit designers do not have access to accurate physics-based aging models to estimate efficient (i.e., small, yet sufficient) guardbands. A machine learning-based aging model are free sensitive material and process parameters of the foundry and can thus be shared with designers. Now, circuit designer can create workload-specific aging data for efficient guardbands.

they overestimate the impact of aging significantly. Today’s high-end devices are operating at the technological limits and cannot afford the unnecessary performance penalties mandated by such pessimistic predictions, an ideal aging model has to be as precise as possible. While physics-based models achieve such high accuracy, they require parameters specific to the manufacturing process to compute the degradation. Such parameters are a valuable secret of the foundry because they reveal details about their technology through material-dependent parameters. The foundry instead provides a process design kit (PDK) covering various corner cases including the worst case (i.e., the slow-slow corner). In summary, designers have limited options to optimize their circuit, which reduces performance and increases costs. An “ideal” aging model should therefore not expose any confidential information about the underlying technology. At the same time, it should still provide accurate estimations, including recovery.

The foundry only guarantees the slow-slow corner leading to very pessimistic guardbands and hence efficiency losses. With the risk of failure on the designers’ side, this pessimism might be reduced. Alternatively, the degradation can be measured during post-silicon validation. However, at this stage, the design is almost complete making changes costly. With an aging model, the impact of the circuit’s workloads and voltages on  $V_{th}$  can be predicted early in the design phase. Starting with the much faster typical-typical corner, an appropriate guardband is added. An ideal aging model is thus available to the designers during design time and allows them to predict the degradation for each individual transistor. During runtime, the remaining guardband can be treated as a resource like remaining battery power. Resource management schemes require a long-term aging model to optimize over the whole lifetime. Physics-based models are not an option, because of their confidential parameters and their high computational complexity. An ideal aging model has a low computational cost to be employed for millions of transistors during design time. At runtime, it provides predictions as a low-overhead background task in the operating system.

### Our Main Contributions

Designers require an *accurate and fast* transistor aging model to optimize the performance of their circuit designs depending on the potential workload. Further, simulating millions and billions of transistors is time consuming necessitating a fast aging model. Physics-based models are slow and confidential, i.e., not accessible to designers. Therefore, we propose to employ machine learning (ML) to model transistor aging. As shown in Fig. 2, the foundry employs its confidential physics-based models to train an ML-based model. Such a model is fast and does not reveal the technology and material parameters. Hence, it can be provided to the circuit designers. They employ the model in conjunction with their workloads to generate their workload-specific, aging-aware PDK. With this PDK, guardbands can be reduced increasing performance.

In this paper, we investigate for the first time how physics-based models can be abstracted through ML methods. ML algorithms like deep neural network (DNN) or long short-term memory (LSTM) have a high computational complexity but can achieve in high accuracy in many applications. As a less computational-intense algorithm, lightweight brain-inspired ML methods have attracted the interest of the community in recent years. Brain-inspired hyperdimensional computing (HDC) does not utilize networks of neurons but is built around large randomly-generated hypervectors [4]. The accurate yet complex equations of physics-based models have to be replaced by a trained ML model. To this end, we investigate two challenges. First, the capability to construct a  $\Delta a V_{th}$  trace from a voltage activity waveform. Such traces and waveforms are typically in the range of nanoseconds to minutes and model short-term aging [5]. Second, predict only the last degradation  $\Delta V_{th}$  value for a single transistor based on a given short voltage activity waveform. This prediction is essential for an extrapolation to ten years until the end of lifetime (EoL) of the device. We investigate the accuracy of the ML models not only on their prediction of this  $\Delta V_{th}$  value. We also employ the predicted  $\Delta V_{th}$  further to extrapolate the circuit delay after ten years and compare the impact on the delay. The performance of the

models is evaluated by training on the transistors of standard cells and an 8-bit adder. The test set are the transistors of a 32-bit MAC unit with which we also evaluate the prediction of the delay after 10 years.

## II. RELATED WORK AND BACKGROUND

Transistor aging has been studied for many years and the impact is well understood. This sections aims at summarizing this research briefly.

### A. Transistor Aging Models

Since manufacturing technology has moved past 45 nm, new materials had to be used [6]. Hafnium Oxide ( $\text{HfO}_2$ ) is used as a high- $\kappa$  dielectric and replaced the traditional silicon dioxide. A drawback of  $\text{HfO}_2$  is its higher number of pre-existing defects in the material itself, making it more susceptible to degradation and thus less reliable. Hence, transistor aging has become a major consideration in modern circuits.

In this work, we focus on NBTI as the primary aging mechanism [2]. Note that our method can be applied analogously to other aging mechanisms like hot carrier degradation (HCD). NBTI aging occurs when the pMOS transistor is turned on. During the on-time, two effects come into play. First, positively charged holes are trapped inside the  $\text{HfO}_2$  dielectric. This increases the  $V_{th}$  of the transistor. If the stress is reduced, i.e., the voltage lowered or the transistor completely turned off, then the holes can be removed and the initial  $V_{th}$  can be recovered over time. Due to the second effect, new traps are generated in the interface material. If the transistor is turned on, these traps are positively charged increasing the  $V_{th}$ . Similar to the first effect, some of these traps may be deactivated once the stress is reduced or removed partially restoring  $V_{th}$ . In both cases  $\Delta V_{th}$  is dictated by the applied voltage.

Most models (especially analytical models) consider recovery only at 0 V. However, measurements have proven that even a reduction in the voltage starts the recovery [3]. The phenomenon is demonstrated in Fig. 1, in which a physics-based NBTI model is employed to calculate the transient trap occupancy, among others [2]. Hence, it is indispensable to consider the dynamics of different voltage levels when modeling aging [7].

ML-based methods to model and predict the impact of aging have been investigated at different levels of the stack. At the system level, reinforcement learning-based methods have been used to schedule threads on a multi-core CPU to reduce aging [8]. At the circuit level, the increase in path delay due to an increased  $\Delta V_{th}$  has been modeled with multivariate adaptive regression splines and compared against support vector machine (SVM) and recurrent neural network (RNN) [9]. Their model takes changing operation conditions, like different voltages, into account. At the gate level, the generation of reliability-aware cell libraries through ML has been demonstrated [10]. In [11], at device level, a single transistor is subjected to constant voltage stress and the  $V_{th}$  curve is fitted with a regression model. In this work, we are the first to explore the applicability of ML methods at the device and physics level. In contrast to [11], we include voltage dynamics and recovery effects. Further, the input to our model is not a single fixed voltage or a statistical

assumption of on/off times, but a trace representing workloads and operating conditions for an individual transistor.

### B. Machine-learning Methods

As for our predictive models, we used different strategies and analyzed what were the trade-offs between each one of them. The multilayer perceptron (MLP) model is one of the simplest neural network models and this practicality has caused its increase on popularity. On the other hand, ML focused on the maximization (support) of separating the margin between classes (vector), also called SVM learning, is a powerful classification tool that has been used widely on many applications and achieved great results.

RNNs are frequently used in application involving sequential data, which fits the temporal nature of aging. However, RNNs frequently fail to learn the important information from the input data involving learning long-term dependencies. By introducing gate functions into the cell structure, the LSTM is able to handle the problem of long-term dependencies well [12]. Since its introduction, almost all the results based on RNNs have been achieved by LSTMs. The many applications include machine translation, time series prediction, natural language processing, and Computer Vision among others [13]. Because of the influence of previous voltages on aging, LSTM's ability to successfully train on data with long-term temporal dependencies makes it natural choice for this application [14].

### C. Brain-Inspired Hyperdimensional Computing

Brain-inspired HDC is a lightweight alternative to traditional ML approaches. It is a rapidly emerging concept that has been successfully applied to voice recognition [15], and hand gesture identification [16], seizures detected [17], image classification [18], pattern recognition for wafer defect maps [19], circuit reliability estimation [20, 21], and others. Implementations range from low-power embedded devices [22] to high-power GPUs [23]. HDC is based on the concept of hypervectors, vectors with thousands of dimensions. The hypervectors can consist of simple bits, integers, real numbers, or other symbols.

Hypervectors representing real-world values (e.g., 0.7 V) are generated once and stored in the item memory. If the same value has to be mapped into hyperdimensional space again, the previously generated item hypervector is retrieved from the item memory. Due to the high dimension, it is very likely that two randomly-generated hypervectors are orthogonal to each other. For binary hypervectors, this similarity metric is computed with the Hamming distance, for integer-based hypervectors using the cosine similarity.

Multiple item hypervectors are combined into a class hypervector through the basic operations of bundling and binding [4]. This process is also called encoding. A voltage waveform is encoded into a single hypervector which then represents said waveform. If a similar waveform is encoded, then its resulting hypervector has a high similarity to the first hypervector. Each operation is executed on the individual independent components of the hypervector making them trivial to parallelize.

Traditional ML methods such as DNN require huge amounts of data and lots of processing power for training [15]. HDC promises to reduce these requirements. Learning from few samples has been demonstrated for the example of seizure detection [24]. The distributed design of hypervectors makes HDC very robust against failures in the underlying memory and thus well suited for less reliable low-power emerging memories [25]. The design makes it also robust against noise in the data, e.g., from low-quality aging monitors embedded in the circuit. Additionally, HDC operations are trivial to parallelize to make use of multiple processing units. All these properties suggest that an ideal aging model can be implemented with HDC.

### III. EXPERIMENTAL SETUP

To evaluate the impact of transistor aging on a circuit, the analysis starts at application level. The activities of the application generates the stimuli for the inputs of the circuit (a NAND gate in this example) as shown in Fig. 2 ①. Those stimuli are then propagated to the individual transistors in ②. In larger circuits, not every transistor is connected to an input and thus its stimulus depends on the logic inside the circuit. Therefore, the circuit has to be simulated to extract the voltage waveforms. In ③, the waveforms are provided as an input to the aging models which generate the corresponding degradation trace. Based on this short-term trace, the EoL degradation is extrapolated, typically to ten years ④. The resulting EoL  $\Delta V_{th}$  for each transistor is applied to the circuit ⑤ and causes an increase of the propagation delay or latency. Only if this aging-induced shift is considered during design can the system continue functioning properly over its whole lifetime.

This work builds on top of the CARAT framework [26] to simulate circuits with SPICE, extract the voltage waveforms, run the aging models, and simulate again to determine the additional propagation delay. A circuit designer can have access to such a framework except for the aging models, which contain sensitive parameters that the foundry does not share. Consequently, the whole flow does not benefit the

designer because they do not know how much guardband each transistor requires. To explore the problem space, the state-of-the-art physics-based BTI Analysis Tool (BAT) framework [2] is employed. It estimates the impact of NBTI on different transistor technologies and manufacturing processes. BAT has been validated against several technologies including FinFET, FD-SOI, and nanosheets. It models the generation of interface and bulk oxide traps as well as hole trapping and other aging effects, including recovery. The model has been calibrated with experimental measurements to obtain the otherwise confidential parameters. Such an effort is infeasible for most designers and not possible for technologies in the early prototype stage. Training data is generated from simple circuits like XOR and NAND. For all our experiments, the temperature is constant at 90 °C. We discuss other temperature values in Section VI. The operating voltage is set to 0.7 V.

In this work, the traditional ML-method SVM and the emerging brain-inspired HDC are investigated. The training data is presented to both methods as described in Section III-B. SVM is based on statistical learning frameworks. Training samples are assigned to one of two groups. To support more classes (i.e., more fine-grained  $\Delta V_{th}$  values), the problem is mapped to multiple binary classifications. The employed Scikit-learn library provides an SVM written in C. An SVM can be extended to a nonlinear classifier using the kernel trick. We perform a grid search to find the best model parameters and utilize the SVM implementation of the Scikit-learn library [27]. The core parts have been implemented in C.

The recently-proposed OnlineHD is selected as an HDC implementation [23]. It uses the MAP-B hypervector architecture [28], in which  $-1$  and  $1$  are the vector components. The distance between two hypervectors is computed with the cosine similarity. OnlineHD supports retraining to increase the prediction accuracy. During retraining, the model is queried with the training dataset and if the prediction is incorrect, the class hypervector is slightly altered to be more similar to the query hypervector. In this work, the number of retraining

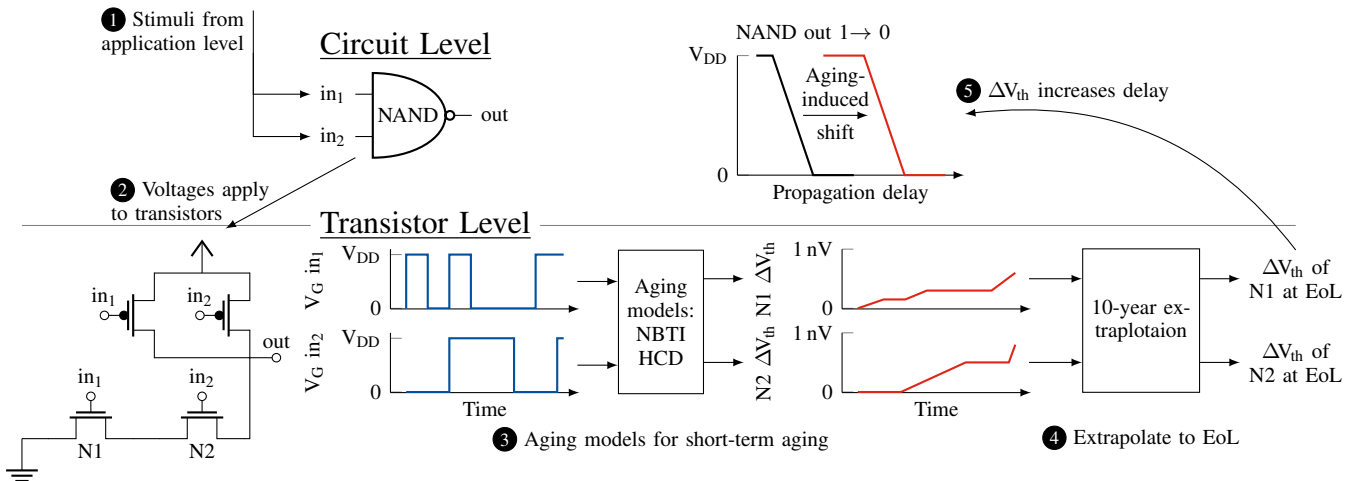


Fig. 3. In the experimental setup, stimuli are applied at circuit level ① and voltage waveforms for each transistor extracted ②. Those are passed to the aging models ③ to generate the ground truth for the training of the machine learning models. Then, their prediction is extrapolated to the end of lifetime (EoL) ④. Finally, the degradation is applied again at circuit level for efficient guardband estimation ⑤.

iterations (epochs) is set to 50 and the learn rate to 0.01. Similar to SVM, major parts of OnlineHD have been implemented in C through PyTorch.

In addition, an LSTM model is implemented as an alternative method to the history-based approach with SVM and HDC. LSTM models have been shown to work well in sequence to sequence learning applications such as translation tasks [29]. In this work, an LSTM encoder-decoder model is trained to predict the full trace based on the input waveform. The encoder contains two layers of stacked LSTMs, each with 256 units, which learn to map the input waveforms to an internal fixed-size vector representations of size 256. The decoder is a one layer LSTM with 256 units. The decoder is trained to map the fixed internal vector to the degradation trace. Similar to [29], the performance of the LSTM model is improved by reversing the input waveforms.

The LSTM model's performance improved as the number of layers and units in each layer increased, as did the model's complexity. It was observed that model tends to overfit when the number units is increased above 256. The LSTM model's performance tends to deteriorate when the number of segments in the input waveform is greater than 32.

This allows for a fair comparison of the computational demands of both methods and against the physics-based BAT, all running on an AMD Ryzen 9 3950X .

#### A. Dataset Generation

Circuit designers have access to foundry-provided PDKs to create and tune their systems. Typically, the foundry publishes an additional set of PDKs with aging data under worst-case conditions, which lead to an overestimated guardband. Actual workloads are far from such worst-case conditions. Therefore, aging models take the workload into account to predict the expected degradation at EoL for a single transistor. The input to the aging model is a waveform  $(V_1, \dots, V_l)$  which is a sequence of  $l$  segments where each segment  $V_i$  with  $i \in \{1, \dots, l\}$  represents the gate voltage applied to the transistor. The supply voltage can be any of the voltage corners provided by the foundry  $V_i \in V_{corners}$ . The time component is included in the waveform through the segment index, with each segment lasting the same amount of time.

The waveform is provided to the aging model, which produces a trace  $(\Delta V_{th,1}, \dots, \Delta V_{th,l})$  reporting a  $\Delta V_{th}$  for each segment. The effect of the input voltage is reflected in the output trace  $V_i \rightarrow \Delta V_{th,i}$ . However, simply using this mapping as a model does not reflect the voltage dynamics and cannot capture recovery effects. The  $\Delta V_{th,i}$  of segment  $V_i$  depends also on the previous segment's  $V_{i-1}$ , as shown in Fig. 1.

Physics-based models can take the whole waveform and compute the expected  $\Delta V_{th}$  for each point in time. To make such a model accessible to the designer, it has to be replaced with a similarly behaving ML-based model to not disclose the confidential technology parameters. Physics-based models retain the state of the transistor (e.g., the number of defects in the material) during the prediction, which is the basis for their powerful predictive capabilities. In contrast, lightweight ML-based methods do not have such an internal state and have to predict  $\Delta V_{th}$  iteratively.

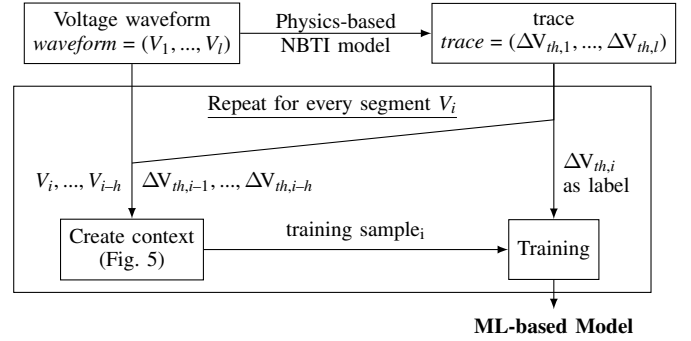


Fig. 4. Voltage waveforms derived from circuit-level stimuli are supplied to the physics-based transistor aging model to create training data for the machine learning-based models. Once they are trained, they take voltage waveforms and predict the degradation trace.

#### B. Training data generation

Training data is generated from 62 standard cells (e.g. XOR, full adder). The cells employed in this work have at most five input terminals and no internal state. With the design of digital circuits in mind, those input terminals are either at 0V or at  $V_{DD}$ . Random stimuli are applied, which in turn stimulate the internal transistors. Through SPICE simulations, the analog waveform for each transistor can be extracted. The physics-based aging model is then executed to compute the corresponding trace. The trace represents the label for a waveform. Depending on the type of the cell, each standard cell contains between 4 and 27 pMOS check transistors. In total, all standard cells contain 414 pMOS transistors. Thus, 414 waveform-trace pairs, the training samples, can be generated.

While the design of the standard cells is well known, the designer's circuits is their intellectual property that cannot be shared with third parties like the foundry. Therefore, we mimic the application scenario for a circuit designer and generate the test set from transistors in larger circuits. In this work, two circuits are explored. First, an adder for two 8-bit numbers with 111 transistors. Second, a 32-bit MAC unit, that multiplies an 8-bit weight with an 8-bit input and accumulates the result with a 32-bit partial sum. The circuit contains 1395 pMOS transistors. The inputs of each circuit are stimulated with random data for an unbiased evaluation. A circuit designer would simulate their typical workload patterns. Similar to the standard cells, the inputs propagate through the circuit and waveforms for each transistor are extracted. In other words, the designer extracts waveforms representing their workload. For evaluation purposes, the physics-based aging model is employed again to compute the traces as a ground truth. The number of consecutive addition or MAC operations can be set to generate waveforms of various lengths. The longer the trace, the more it challenges the ML model since more features (input voltages) have to be considered.

### IV. SCENARIO 1: PREDICTING A FULL TRACE

The objective is to predict a  $\Delta V_{th}$  for each segment of the waveform. In contrast to an LSTM, an SVM or an HDC cannot directly convert a sequence to another. Hence, the waveforms have to be processed to make them learnable by the latter



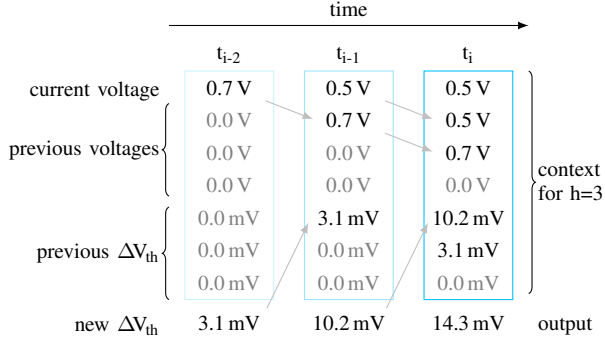


Fig. 5. Some history is added to the current input voltage to better capture the voltage dynamics. In this example  $h = 3$ , i.e., the input voltage and  $\Delta V_{th,i}$  from  $t_{i-1}$ ,  $t_{i-2}$ , and  $t_{i-3}$  are included.

models. The training procedure for one waveform is sketched in Fig. 4. Since the current state of the transistor is not available for training, the voltage dynamics have to be captured with a history of  $h$  previous waveform segments. However, such a snippet of the waveform sequence is not bound to a specific point in time or, more importantly, to the current internal state of the transistor. Setting  $h = 1$  (i.e., include all segments) is not viable due to the prohibitively large parameter space. Thus, a history of the  $h$  previous  $\Delta V_{th}$  values is included as well. The combination of voltage and  $\Delta V_{th}$  provides a more detailed context for training. Fig. 5 visualizes the information contained in three training samples for  $h = 3$ . The label for each sample at time  $i$  is the  $\Delta V_{th,i}$  of the segment taken from the trace. The  $\Delta V_{th,i}$  is quantized to discrete labels for classification.

The results show that the SVM and HDC models have a bias in their predictions. Although their predictions follow the traces in general, the nominal  $\Delta V_{th}$  values often deviate. A multiplier can reduce this offset. After the model training is complete, it is used on the training set itself to predict the traces. The disagreement between the ML-based and the physics-based model is analyzed and the resulting average deviation is used as a multiplier during inference.

#### A. Inference

During inference, the same data representation, described above, is used for SVM and HDC. This representation includes the  $h$  previous  $\Delta V_{th}$ . However, only the waveform is available during inference. Hence, the  $\Delta V_{th}$  values have to be predicted online during inference. They are then adjusted with the multiplier to be directly used to predict the next segment. For the first segment  $i = 1$ , the initial  $\Delta V_{th}$  and the “previous”  $\Delta V_{th}$  is set to 0 mV, as shown in Fig. 5. In effect, only the input voltage  $V_1$  determines  $\Delta V_{th,1}$ . The predicted  $\Delta V_{th,1}$  is then used to create the context for segment  $i = 2$ ,  $\Delta V_{th,1}$  and  $\Delta V_{th,2}$  for segment  $i = 3$ , and so forth. Due to this recursive process, prediction errors multiply requiring high precision.

#### B. Evaluation

The performance of the ML-based models under a variety of different aspects is evaluated. The datasets are generated and

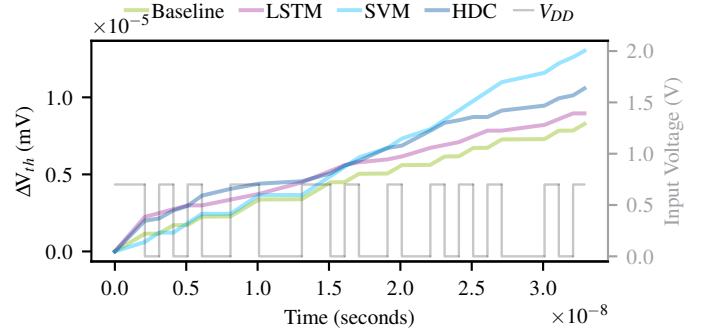


Fig. 6. Example of a waveform (gray), the baseline trace from the physics-based model (green) and the predicted traces from various ML models.

split into training and testing set with a 70 % split. As a metric, the relative error per segment  $RE_i = (ML_i - BAT_i) / BAT_i * 100\%$  is used.  $ML_i$  and  $BAT_i$  are the predictions for segment  $i$  from the ML-based and physics-based models, respectively. The difference is divided by  $BAT_i$ , the final  $\Delta V_{th}$ . Overestimating the degradation results in a positive  $RE$ , underestimating it in a negative. The results in Fig. 7 show balanced models with a tendency for overestimation.

#### C. Dimension of the HDC Model

The dimension of the hypervectors determines their capacity to store information. The higher the dimension, the higher the expected accuracy. This increase levels off at an application-specific point, which is not known a priori. A higher dimension also correlates with more costly operations and higher memory requirements. Both costs are not the primary concern during design time. Therefore, HDC-based models with high dimensions above 10,000 are feasible.

In this work, dimensions from 1000 to 20,000 vector elements are explored. Contrary to the initial assumption, a higher dimension does not necessarily result in higher accuracy. The mean  $RE$  for different dimensions is shown in Fig. 8. The highest dimension of 20,000 performs best on average over different  $h$ , but even the lowest dimension with 1000 outperforms others. These results indicate that the HDC model has unused capacity available.

#### D. Impact of History $h$

The parameter  $h$  determines how many previous segments are taken into account to predict the next segment. The SVM performs best with  $h = 8$ . For HDC, the combination with the dimension has to be considered. More history requires a higher capacity of the model to contain the information. While this capacity is available with the high dimensions, the results suggest an oversaturation of the query hypervector with the same voltage hypervector. A different encoding is expected to mitigate this issue. The overall best performances for HDC are achieved with  $h$  around seven.

The hyperparameters dimension and  $h$  can be selected based on the model’s performance on the training data. Our analysis of circuits, discussed in Section V, shows that different settings are required depending on the workload characteristics. The best model is selected by the foundry and sent to the designer.

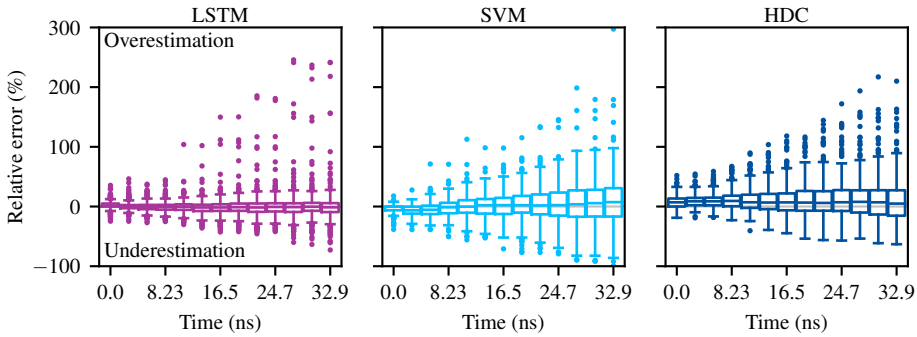


Fig. 7. The SVM and HDC models rely on their own previous outputs for the next prediction. Hence, the error accumulates, which is represented by the increase in the relative error. The LSTM directly translates the whole sequence and achieves a higher accuracy although outliers are as bad as in other models. Training and test are performed on the adder circuit.

TABLE I  
EXECUTION TIMES FOR THE 8-BIT ADDER CIRCUIT.

Task		Wall-clock time
Training set generation	(total)	409.0 s
HDC training	(total)	34.2 s – 152.3 s
SVM training	(total)	407.7 s
Physics-based trace prediction	(mean)	602.2 ms
HDC trace prediction	(mean)	28.7 ms – 88.1 ms
SVM trace prediction	(mean)	624.1 ms
LSTM trace prediction	(mean)	1006.7 ms

### E. Reduction of Model Execution Time

In the HDC model, the complex differential equations of the physics-based model are replaced with simple operations on integer vectors. The performance advantages are reflected by a reduced execution time shown in Tab. I. Predicting a 32-segment trace for the 8-bit adder takes 29 ms to 88 ms for a dimension of 1000 and 20,000, respectively. This is up to 30X faster compared to the physics-based model with 602 ms or the SVM with 624 ms. The time for training varies with  $h$ , but it is consistently lower for the HDC model compared to the SVM. OnlineHD utilizes multiple CPU cores to reduce the training time. The LSTM takes the most time, even longer than the physics-based model, but achieves the best accuracy.

## V. SCENARIO 2: END-OF-LIFETIME AGING

Recreating the degradation trace is useful in evaluating short-term aging effects [5]. To predict the degradation at the EoL of the device, and thus for circuit designers to add sufficient guardbands, the whole trace is not necessary. The extrapolation model for NBTI considers the waveform as well as the last  $\Delta V_{th}$  value. Hence, an ML model is sufficient for EoL  $\Delta V_{th}$  estimation if it can predict this last value. Consequently, the challenge transforms from a recursive trace reconstruction to a simpler regression. With the focus on long-term aging, the final impact of inaccurate predictions from ML models can be evaluated at circuit level. The physics-based BAT is replaced with an ML model to provide the short-term aging value. This result is then processed further by the CARAT framework to predict the aging-induced shift in the circuit’s propagation delay.

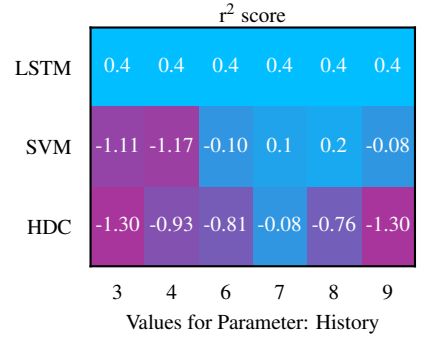


Fig. 8. Mean  $r^2$  scores for different histories  $h$  with an HDC dimension of 20k for the adder dataset.

### A. Model Training and Evaluation

Many ML algorithms exist to solve regression problems. The input is a waveform, where each segment acts as a feature and the predicted output is the last  $\Delta V_{th}$  value.

An SVM can also be used for regression and is then referred to as an **SVR**. The implementation is based on the Scikit-learn library [27] and a grid search is done for hyperparameter tuning. The SVR has an Radial Basis Function kernel, a gamma value of 0.001, and a C of 100. An **MLP** is implemented with PyTorch [30]. It has a total of three layers with 128 neurons in the hidden layer. The output layer is a single neuron. In contrast to classification, this single neuron returns a floating point value representing the last  $\Delta V_{th}$ . An **HDC** classifier can be used for regression by quantizing the  $\Delta V_{th}$  values and treating those as classes. For comparison, a **worst-case model** is created. With NBTI, the pMOS transistor ages if no gate voltage is applied. Hence, the worst case assumes that the transistor is turned off and only turns on at the end of the simulated time frame to maximize the aging effect.

Each model is trained and evaluated on three circuits. The dataset generation is described in detail in Section III-A. The aging extrapolation models for NBTI depend on the last  $\Delta V_{th}$  value and the waveform. But instead of the physics-based aging model, the ML models are employed. The predictions are compared with the output of the physics-based model as a baseline. As an accuracy metric,  $r^2$  score is select, with a value of ‘1’ as a perfect match.

### B. Results at Circuit Level

To judge the complex of the problem, the models are trained and tested on the adder circuit. Three sets of random inputs are generated for training, hyperparameter tuning, and testing. The results are presented in Fig. 9 and show the correlation between the baseline physics-based last  $\Delta V_{th}$  values and the ML-based ones for all transistors. The  $r^2$  scores are given above the plots and show that the best ML approach is the LSTM model. An  $r^2$  score of 0.37 was achieved with a training for 500 epochs, two hidden layers with 25 units per layer, and the L1 loss function. Although there is some spread around the baseline, the model’s ability to predict the  $\Delta V_{th}$  is clear. A similar picture is given by the MLP, the predictions are

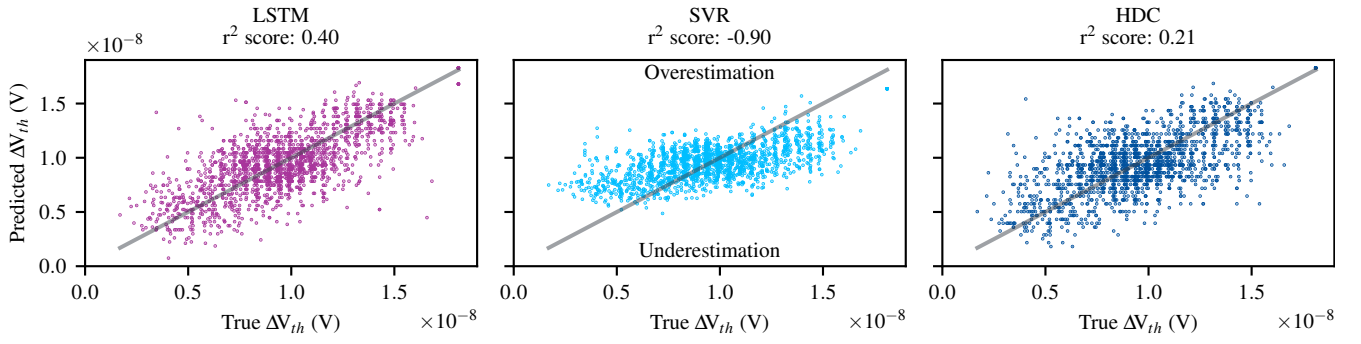


Fig. 9. Training and testing on the same circuit provides a baseline for the complexity of the problem to predict the final  $\Delta V_{th}$  value based on the trace. The LSTM predicts the whole trace but only the last value is considered in the evaluation.

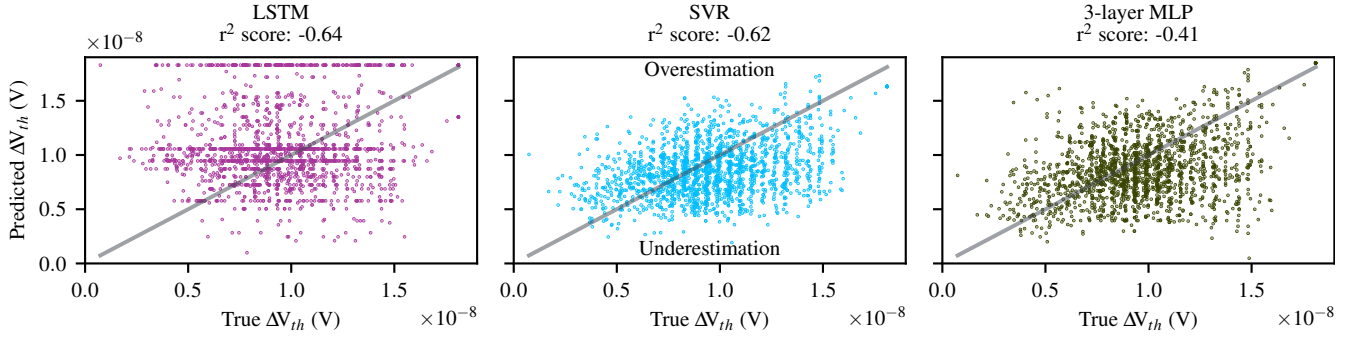


Fig. 10. Standard cells are provided by the foundry and the base for many circuit designs. However, the training dataset generated from them is too small for the ML methods to sufficiently learn and generalize. Hence, the inference results with the adder circuit are worse compared to Fig. 9.

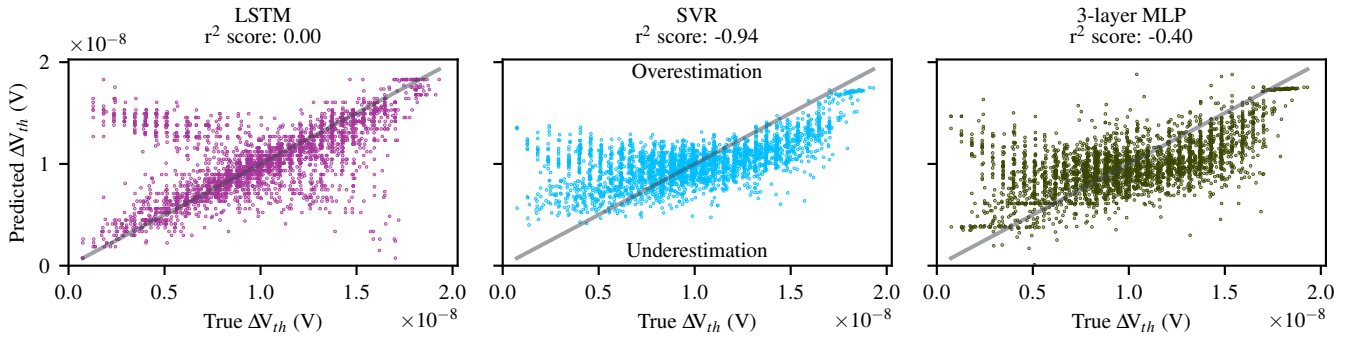


Fig. 11. The models are trained on the adder circuit and used to predict the degradation in the MAC circuit. The large dataset from the adder allows the LSTM to train and provide adequate results. The outliers are analyzed in Section V-C.

correlated with the baseline values. For HDC, the spread is even larger but still follows the baseline. The model is trained with a dimension of 4000 for 50 epochs.

While HDC has the highest spread, the mean aging-induced shift in the propagation delay at circuit level is equal to the baseline. Tab. II compares the different models and also includes the worst-case model with constant aging stress. Both, HDC and MLP, overestimate the impact overestimate aging, which is preferable to the LSTM, which underestimates the impact and thus could lead to insufficiently small guardbands. However, even with doubling the ML-based predictions to save guard against underestimation, the ML-models still outperform the worst-case model by a factor of three.

Training and predicting for the same circuit would require that the circuit designers share details with the foundry, which would train the model. To minimize data sharing, the foundry

can train a model on their standard cells and provide those models to designers. However, the results plotted in Fig. 10 show a significant degradation of the quality of the predictions. The  $r^2$  scores drop below zero and the models struggle to generalize. Worse, the LSTM and the MLP predict low  $\Delta V_{th}$  values although the baseline values are close to the maximum (prediction in lower right corner). While the spread of the SVM has increased compared to a training with the adder, the maximum prediction errors are smaller than with other ML models. The HDC model has failed to generalize and is not included in the results.

Similar and better results are shown in Fig. 11 for training on the adder and testing on the MAC circuit. First, the LSTM has sufficient data to train and can predict most samples with a low error. Nevertheless, outliers can cause incorrect guardband estimations. Second, while the SVM's  $r^2$



TABLE II  
AGING-INDUCED DELAY FOR TRAIN AND TEST ON ADDER CIRCUIT.

Delay (ps)	Baseline	LSTM	SVR	HDC	Worst Case
min	-2.08	-2.08	-0.40	-1.81	-2.12
mean	4.88	4.66	5.33	4.88	31.36
max	12.60	11.70	11.70	13.90	61.10

TABLE III  
AGING-INDUCED DELAY FOR TRAIN ON STANDARD CELLS AND TEST ON ADDER CIRCUIT.

Delay (ps)	Baseline	LSTM	SVR	MLP	Worst Case
min	-2.08	-4.33	-0.93	-1.14	-2.13
mean	4.76	6.76	5.06	5.19	31.52
max	10.90	18.80	12.60	15.10	61.10

is the lowest, it underestimates the least preventing severely incorrect guardband estimations. Overestimations are limited to smaller  $\Delta V_{th}$  values and in total the SVM model achieves a mean relative error of 1.7% compared to the LSTM's 3%. Finally, the largest  $\Delta V_{th}$  value in the MAC dataset is higher than in the adder and this behavior is not captured by the ML models, they are limited by their training. This is evident by the horizontal cluster in the top right.

### C. Error Analysis

While many predictions of the LSTM are within a tolerable error range, there are outliers that are either under- or overestimated as shown in Fig. 11. The same samples are plotted in Fig. 12 for an error analysis. First, overestimated samples have a lower duty cycle and especially fewer voltage transitions in the waveform. In other words, transistors that are off most of the time and change their on/off state seldom. Overestimations have a negative impact on the circuit's timing because guardband are designed unnecessary large. However, they do not lead to failure of the device, in contrast to underestimations. The impact of aging is underestimated for some transistors with a duty cycle above 0.6. Their waveforms have an average amount of transitions. This combination of duty cycle and number of transitions is not a defining feature for underestimations by the LSTM model. Hence, it is impossible to derive a simple rule-based solution to contain the potential timing errors due to insufficient guardbands.

The SVR shows a similar pattern. Overestimations correlate with a low duty cycle combined with a low number of transitions in the waveform. Underestimations are not as frequent and as pronounced. While they occur mainly above a duty cycle of 0.4, worst-case underestimations do not correlate with the number of transitions in the waveform. Hence, similar to the LSTM, a simple rule-based error reduction cannot be derived. In summary, the models perform well for most samples but outliers, especially underestimations, still pose a challenge.

## VI. DISCUSSION

The focus of this work is on NBTI, the dominant degradation effect in current transistor technology [2]. Nevertheless, PBTI and HCD also play an important role. Their impact on the

TABLE IV  
AGING-INDUCED DELAY FOR TRAIN ON ADDER AND TEST ON MAC CIRCUIT.

Delay (ps)	Baseline	LSTM	SVR	MLP	Worst Case
min	-1.80	-2.90	-2.10	-3.80	-70.70
mean	5.03	5.58	5.31	4.94	88.67
max	15.00	14.90	12.60	11.50	450.91

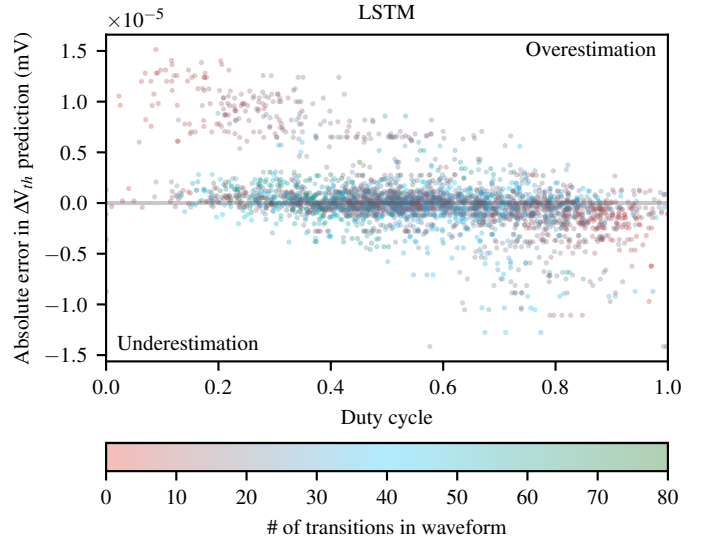


Fig. 12. Analysis of the LSTM model for the MAC circuit. The largest prediction errors are correlated with a low duty cycle and a low number of voltage transitions.

transistor has to be considered as well to design the circuit with small yet sufficient timing guard bands. Hence, an investigation into replacing those models with ML-based models is necessary. Preliminary results suggest that the methods explored in this work are challenged by the different types of stimuli driving those degradation effects. In NBTI, the on/off time is the dominant factor whereas in HCD the number of transitions has to be considered, among other stimuli.

Aging effects also depend heavily on the temperature of the transistor. The experiments in this work assume a constant temperature of 90 °C. However, the temperature of a transistor keeps changing between high-load phases and standby states of the overall system the circuit is integrated in. Those dynamic changes have to be investigated and included for a temperature-aware ML-based trace prediction.

## VII. CONCLUSION

Accurate physics-based aging models include confidential technology and material parameters. Thus, such models are not available to circuit designers to optimize their designs under the actual impact of aging. This work explores the applicability of ML-based methods to train on the physics-based models, in particular traditional SVM, LSTM, and brain-inspired HDC. While ML-based models can predict the impact of aging for most transistors accurately, outliers can be over- or underestimated. Nevertheless, the explored ML-based methods predict the degradation about 3x more precise than available worst-case models. For the first time, circuit designers have

access to an accurate aging model which is indispensable for efficient designs. This work opens the door to narrow the boundary between foundry and circuit designers.

#### ACKNOWLEDGMENT

The authors would like to thank Victor van Santen for his support with the physics-based aging models. This research was partially supported by Advantest as part of the Graduate School “Intelligent Methods for Test and Reliability” (GS-IMTR) at the University of Stuttgart.

#### REFERENCES

- [1] D. S. Huang, J. H. Lee, Y. S. Tsai, Y. F. Wang, Y. S. Huang, et al., “Comprehensive device and product level reliability studies on advanced CMOS technologies featuring 7nm high-k metal gate FinFET transistors,” in *2018 IEEE international reliability physics symposium (IRPS)*, 2018, 6F.7–1–6F.7–5.
- [2] S. Mahapatra and N. Parihar, “Modeling of NBTI using BAT framework: DC-AC stress-recovery kinetics, material, and process dependence,” *IEEE Transactions on Device and Materials Reliability*, vol. 20, no. 1, pp. 4–23, 2020.
- [3] S. Satapathy, W. H. Choi, X. Wang, and C. H. Kim, “A revolving reference odometer circuit for BTI-induced frequency fluctuation measurements under fast DVFS transients,” in *2015 IEEE International Reliability Physics Symposium, IRPS 2015*, 1, 2015, 6A31–6A35.
- [4] P. Kanerva, “Hyperdimensional computing: An introduction to computing in distributed representation with high-dimensional random vectors,” *Cognitive Computation*, vol. 1, pp. 139–159, 2009.
- [5] V. M. van Santen, H. Amrouch, J. Martin-Martinez, M. Nafria, and J. Henkel, “Designing guardbands for instantaneous aging effects,” in *2016 53rd ACM/EDAC/IEEE Design Automation Conference (DAC)*, IEEE, 2016, pp. 1–6.
- [6] J. Keane and C. H. Kim, “Transistor aging,” *IEEE Spectrum*, vol. 48, no. 5, pp. 28–33, 2011.
- [7] V. M. van Santen, H. Amrouch, N. Parihar, S. Mahapatra, and J. Henkel, “Aging-aware voltage scaling,” in *2016 Design, Automation Test in Europe Conference Exhibition (DATE)*, 2016, pp. 576–581.
- [8] A. Das, R. A. Shafik, G. V. Merrett, B. M. Al-Hashimi, A. Kumar, et al., “Reinforcement learning-based inter- and intra-application thermal optimization for lifetime improvement of multicore systems,” in *2014 51st ACM/EDAC/IEEE Design Automation Conference (DAC)*, 2014, pp. 1–6.
- [9] K. Huang, X. Zhang, and N. Karimi, “Real-time prediction for IC aging based on machine learning,” *IEEE Transactions on Instrumentation and Measurement*, vol. 68, no. 12, pp. 4756–4764, 2019.
- [10] F. Klemme and H. Amrouch, “Machine learning for on-the-fly reliability-aware cell library characterization,” *IEEE Transactions on Circuits and Systems I: Regular Papers*, vol. 68, no. 6, pp. 2569–2579, 2021.
- [11] N. Chatterjee, J. Ortega, I. Meric, P. Xiao, and I. Tsameret, “Machine learning on transistor aging data: Test time reduction and modeling for novel devices,” in *2021 IEEE International Reliability Physics Symposium (IRPS)*, 2021, pp. 1–9.
- [12] S. Hochreiter and J. Schmidhuber, “Long short-term memory,” *Neural Comput.*, vol. 9, no. 8, pp. 1735–1780, 1997.
- [13] A. R. Priatama and Y. Setiawan, “Regression models for estimating aboveground biomass and stand volume using landsat-based indices in post-mining area,” *J. Manaj. Hutan Trop. (J. Trop. For. Manag.)*, vol. 28, no. 1, pp. 1–14, 2022.
- [14] S. Hochreiter and J. Schmidhuber, “Lstm can solve hard long time lag problems,” in *Advances in Neural Information Processing Systems*, vol. 9, MIT Press, 1996.
- [15] M. Imani, D. Kong, A. Rahimi, and T. Rosing, “VoiceHD: Hyperdimensional computing for efficient speech recognition,” in *2017 IEEE Int. Conf. on Rebooting Computing (ICRC)*, 2017, pp. 1–8.
- [16] A. Moin, A. Zhou, A. Rahimi, S. Benatti, A. Menon, et al., “An EMG gesture recognition system with flexible high-density sensors and brain-inspired high-dimensional classifier,” in *2018 IEEE International Symposium on Circuits and Systems (ISCAS)*, 2018, pp. 1–5.
- [17] A. Burrello, S. Benatti, K. A. Schindler, L. Benini, and A. Rahimi, “An ensemble of hyperdimensional classifiers: Hardware-friendly short-latency seizure detection with automatic iEEG electrode selection,” *IEEE Journal of Biomedical and Health Informatics*, pp. 1–1, 2020.
- [18] Y.-C. Chuang, C.-Y. Chang, and A.-Y. A. Wu, “Dynamic hyperdimensional computing for improving accuracy-energy efficiency trade-offs,” in *2020 IEEE Workshop on Signal Processing Systems (SiPS)*, 2020, pp. 1–5.
- [19] P. R. Genssler and H. Amrouch, “Brain-inspired computing for wafer map defect pattern classification,” in *IEEE International Test Conference (ITC’21)*, 2021.
- [20] H. Amrouch, F. Klemme, and P. R. Genssler, “Design close to the edge in advanced technology using machine learning and brain-inspired algorithms,” in *27th Asia and South Pacific Design Automation Conference (ASP-DAC’22)*, 2022.
- [21] P. R. Genssler and H. Amrouch, “Brain-inspired computing for circuit reliability characterization,” *IEEE Transactions on Computers*, 2022.
- [22] M. Imani, Z. Zou, S. Bosch, S. A. Rao, S. Salamat, et al., “Revisiting HyperDimensional learning for FPGA and low-power architectures,” in *2021 IEEE International Symposium on High-Performance Computer Architecture (HPCA)*, 2021, pp. 221–234.
- [23] A. Hernandez-Cane, N. Matsumoto, E. Ping, and M. Imani, “OnlineHD: Robust, efficient, and single-pass online learning using hyperdimensional system,” in *2021 Design, Automation Test in Europe Conference Exhibition (DATE)*, 2021, pp. 56–61.
- [24] A. Burrello, K. Schindler, L. Benini, and A. Rahimi, “One-shot learning for iEEG seizure detection using end-to-end binary operations: Local binary patterns with hyperdimensional computing,” in *2018 IEEE Biomedical Circuits and Systems Conference (BioCAS)*, 2018, pp. 1–4.
- [25] G. Karunaratne, M. Le Gallo, G. Cherubini, L. Benini, A. Rahimi, et al., “In-memory hyperdimensional computing,” *Nature Electronics*, pp. 1–11, 2020.
- [26] V. M. van Santen, S. Thomann, C. Pasupuleti, P. R. Genssler, N. Gangwar, et al., “Bti and hcd degradation in a complete 32 × 64 bit sram array – including sense amplifiers and write drivers – under processor activity,” in *2020 IEEE International Reliability Physics Symposium (IRPS)*, 2020, pp. 1–7.
- [27] F. Pedregosa, G. Varoquaux, A. Gramfort, V. Michel, B. Thirion, et al., “Scikit-learn: Machine learning in python,” *Journal of Machine Learning Research*, vol. 12, pp. 2825–2830, 2011.
- [28] R. W. Gayler, “Multiplicative binding, representation operators & analogy (workshop poster),” 1998.
- [29] I. Sutskever, O. Vinyals, and Q. V. Le, “Sequence to sequence learning with neural networks,” in *Advances in Neural Information Processing Systems*, vol. 27, Curran Associates, Inc., 2014.
- [30] A. Paszke, S. Gross, F. Massa, A. Lerer, J. Bradbury, et al., “Pytorch: An imperative style, high-performance deep learning library,” in *Advances in Neural Information Processing Systems*, vol. 32, 2019.